

A cryogenic-electron microscopy study of the one-phase corridor in the phase diagram of a nonionic surfactant-based microemulsion system

Irina Davidovich¹ · Liron Issman² · Camila de Paula¹ · Ido Ben-Barak¹ · Yeshayahu Talmon¹

Received: 18 July 2015 / Revised: 15 September 2015 / Accepted: 15 September 2015 / Published online: 5 October 2015
© Springer-Verlag Berlin Heidelberg 2015

Abstract We describe full nanostructural characterization of the “one-phase corridor” in the “ χ -cut” phase diagram of the isooctane-water- $C_{12}E_5$ system. We followed the nanostructural development from oil-in-water microemulsion to a bicontinuous microemulsion, and to water-in-oil microemulsion, as the oil content is increased, and temperature is raised accordingly. We used cryogenic-temperature transmission electron microscopy (cryo-TEM) and cryogenic-temperature scanning electron microscopy (cryo-SEM). In most of the composition range studied, we were able to apply both methodologies with similar results. This is a first report of nanostructural mapping of the entire composition range, from water-rich to oil-rich, of a microemulsion system, using well-controlled cryo-specimen preparation. The nanostructural sequence directly imaged here agrees well with theory and previous experimental work by nonimaging techniques, and some, partial electron microscopy.

Keywords Microemulsions · Nonionic surfactants · Cryo-TEM · Cryo-SEM · Nanostructure

Dedicated to a dear friend and a superb colleague, Prof. Dr. Heinz Hoffmann on his 80th birthday

✉ Yeshayahu Talmon
ishi@tx.technion.ac.il

¹ Department of Chemical Engineering and The Russell Berrie Nanotechnology Institute (RBNI), Technion-Israel Institute of Technology, Haifa 3200003, Israel

² Present address: Tortechn Nano Fibers Ltd., POB 9035 Ma'alot Tarshiha, Israel

Introduction

The term “microemulsion” goes back to the work of Hoar and Schulman [1] who formed a clear “emulsion” of benzene in surfactant micelles, by the addition of a sufficiently large amount of an alcohol. That term has been used to describe a transparent or translucent mixture of oil, water, surfactant, and, sometimes, a “co-surfactant,” such as a short-chain alcohol. However, the term is somewhat misleading: in most cases, the domain sizes in such systems are on the nanometric scale, and strictly speaking, the mixture is not an “emulsion,” which by definition is an unstable or metastable system and is made of droplets of one phase dispersed in another. As is well known now, and as originally suggested by Scriven [2], some of the most interesting microemulsions are not made of droplets of one phase suspended in another, continuous phase, but are bicontinuous. A well-accepted current working definition of microemulsions (MEs) was suggested by Danielson and Lindman [3]: “a system of oil, water, and amphiphile, which is a single optically isotropic, thermodynamically stable solution.” Because of the difficulty to determine “thermodynamically stability,” Friberg [4] suggested to replace the term “thermodynamically stable” in the above definition by “formed spontaneously.” The definition and its modification do not refer to the structure, or, as we would say today, the nanostructure of microemulsions, probably because of the difficulty in the exact determination of that nanostructure. That quite elusive nanostructure is in the center of this paper.

At low oil concentration or at low water concentrations, MEs are swollen micellar or inverse micellar solutions, with micelles that are spheroidal or threadlike (“cylindrical,” “wormlike”) in geometry. As oil or water concentrations are increased, the systems become two-phasic, made of an ME phase coexisting with either an oil-rich or a water-rich phase. At comparable oil and water concentrations, a three-phase

system may form, made of a bicontinuous middle phase in equilibrium with a water-in-oil and an oil-in-water phases. The interfacial tension between the middle phase and the upper or the lower phase can be extremely low, down to 0.01 mN/m. Quite often, a cosurfactant is required to obtain such systems. At some given set of system composition and temperature, a single-phase ME may be formed. In all ME phases, the interface between oil and water domains is stabilized by surfactant (or mixed surfactant) film. These domains are labile and undergo spontaneous fluctuations. The phase diagrams of MEs have been extensively studied experimentally and theoretically. Many of those studies can now be found in standard texts such as Evans and Wenerström's [5]. A good extensive review of the nanostructure of MEs was given by Komura [6].

One could classify MEs according to the surfactants used: either ionic surfactant microemulsions or nonionic surfactant microemulsions. In the case of MEs made of systems of ionic surfactants, excess salt should be added to shield the ion charge on the interfacial oil-water layer. Only a few exception to that rule have been reported [7, 8], notably the dodecane/water/didodecyldimethyl ammonium bromide (DDAB) system [9, 10]. While the phase diagram at room temperature contains a large one-phase region, a fairly high surfactant concentration, around 10 %, is needed to form a 1:1 water-oil ME system.

Other regions of the phase diagram exhibit different macroscopic properties, e.g., viscous and nonviscous, conducting and not conducting regions. A single-phase “channel” going from water- to oil-continuous, through bicontinuous, phases has been reported for a number of microemulsions of nonionic surfactants [11–13]. To remain in such a channel, normally one has to change the system temperature to obtain the right curvature of the amphiphilic monolayer for the given ME phase. The same effect may be brought about by adding a cosurfactant [14]. Recently, we studied a mixture of an anionic and a nonionic surfactant, at varying ratios between the two, to produce such one-phase channel [15]. One of the domains of the phase diagram shows structures that are not unlike high-internal phase emulsion (HIPE [16]), but on the nanometric rather than the micrometric scale.

As mentioned above, temperature affects strongly the phase behavior of a given ME system. Kahlweit and Strey [17] showed “triangular prism” phase diagrams that show well that effect for a series of nonionic surfactant ME systems, defining lower and upper critical temperature for the formation of bicontinuous phases. More recently, Arleth and Pedersen [18] showed the effect of temperature on the nanostructures formed and the domain polydispersity in AOT [bis(2-ethylhexyl)sulfosuccinate sodium salt] MEs, studied by contrast-variation small-angle neutron scattering.

Original interest in MEs started in the mid 1970s, in their application in enhanced oil recovery (EOR), namely, in

producing more oil from oil fields, from which no more oil can be produced by “water flooding.” While this original interest in MEs had waned until recently, increasing oil prices have rekindled interest in MEs for EOR [19, 20]. Oil prices have gone down again, when this article is being prepared. Other applications include drug and nutraceuticals delivery in all types of MEs, as reviewed, e.g., by Spornath and Aserin [21]. Polymerizable MEs are another interesting possible application [22]. Oil-in-water or water-in-oil MEs are excellent vehicles for solubilizing a component that cannot be readily dissolved in a particular medium, and, as such can be used as nanoreactors [23, 24], or for the synthesis of nanoparticles [25].

To image nanometric domains MEs at supramolecular resolution one should use electron microscopy, either transmission electron microscopy (TEM) or scanning electron microscopy (SEM). These liquid systems of considerable vapor pressure must be made compatible with the high vacuum of the microscope, and all motion on the supramolecular level must be stopped. For cryo-TEM, we need a thin enough specimen. In cryo-SEM, we must ensure electrical neutrality of the cryo-specimen. As in all forms of microscopy, we must have sufficient contrast in the prepared specimens. One should also remember that all complex liquids such as microemulsions are very sensitive to electron radiation damage, that is, ionization and destruction of the specimen by the electron beam even at very short electron exposures [26].

Direct imaging of the entire composition and temperature range of microemulsions was an unreachable goal for a long time. Because microemulsions are very sensitive to small temperature and concentration variations, see, for example, any of the published phase diagrams [27–29], preparing electron microscope specimens that preserve the system is not an easy task. Staining and drying techniques, originally developed for biological systems, cannot be used, because the stains are typically salts or acid of heavy elements, which change the ionic strength of the system. Drying after staining leads to gradual and drastic change of concentration. Thus, we cannot expect nanostructure preservation by such specimen preparation [30]. One also needs to image the nanostructure at a prescribed temperature, another complication of complex liquid systems specimen preparation.

Because of the above, we have chosen physical, not chemical, specimen preparation methodologies [31]. Such methodologies involve very fast specimen cooling to preserve its native structure. The goal is to vitrify, not freeze, the specimen. The liquid becomes a glass (“amorphous ice”), avoiding crystallization artifacts brought about by freezing. Water requires a cooling rates of approximately 100,000 K/s to vitrify [32], while most organic liquids, notably except linear hydrocarbons, can be vitrified by ~5000 K/s cooling rates. The fast cooled specimen is then transferred under controlled conditions into the electron microscope and examined at cryogenic

temperatures. The low temperatures are required to keep the vapor pressure of the specimen way below the vacuum in the microscope and to keep the metastable vitrified phase from crystallizing. This is the basis for either cryogenic-temperature transmission electron microscopy (cryo-TEM) or scanning cryogenic-temperature electron microscopy (cryo-SEM).

To ensure that the entire specimen preparation procedure is carried out in controlled environment of fixed temperature and an atmosphere saturated with the volatile components of the prepared system, we had developed the controlled environment vitrification system (CEVS) [31] for cryo-TEM specimen preparation. Over the years, we have continuously upgraded the CEVS. The current state-of-the-science of cryo-EM is described by Talmon in a recent paper [33].

Cryo-TEM is now applied by many, as can be appreciated from recent review articles [34–36]. Most applications involve aqueous systems, but recently, oil-continuous phases have also been studied by cryo-TEM, from toluene [37] thru edible oils [38] to superacids [39, 40]. Microemulsions have been imaged by cryo-TEM, but they were mostly of the swollen micelle type, e.g., Bernheim-Groswasser et al. [41]. Bicontinuous microemulsions are very difficult to image by cryo-TEM because of the very high interfacial surfactant-rich area between oil and water domains, leading to high sensitivity to electron-beam radiation damage. Also, the inherent contrast between the water and oil phases is low, which further complicates imaging.

Jahn and Strey [33] apparently overcame those difficulties by applying freeze-fracture-replication (FFR), a methodology where a rather thick specimen is cooled by plunging into a cryogen, fractured, and a metal-carbon replica is prepared by “shadowing” the fracture surfaces with a sputtered heavy metal and “backing” by a carbon layer. After thawing the specimen, the replica is retrieved, cleaned, dried, and imaged by TEM at room temperature. Jahn and Strey described systematic study of several microemulsions, showing the progression of their nanostructure. However, the preservation of the native state in the replicas, which were not prepared under fully controlled conditions, was questionable, as the sample was exposed to ambient air for a short time prior to fixation. They also used an unusual contrast mechanism, based on surface decoration of the oil domains, whose mechanism is not clear. Nevertheless, as we show below, they did obtain very good data!

Koetz and coworkers applied cryo-SEM to study a several microemulsion systems [22, 42, 43], but the methodology and equipment they applied did not provide adequate control of the temperature and concentration of the investigated system. Also, they did not conduct a systematic direct-imaging study of the ME phase diagrams. The cryo-SEM methodology developed by our group and described by Issman and Talmon [44] is based on our cryo-TEM methodology, and, as demonstrated, allows us to prepare cryo-SEM specimens of a wide

range of material systems, including MEs and nonaqueous systems [45, 46].

Here, we describe a systematic study, applying both cryo-TEM and cryo-SEM, to follow the nanostructure, as we go from the water-rich side of the phase diagram to the oil-rich side, along the “one-phase corridor” that one observes in the “ χ -cut” of the of the isooctane-water- $C_{12}E_5$ system phase diagram, namely, at a constant surfactant concentration, and increasing relative amounts of oil and of temperature. To image microemulsions, labile systems that are very sensitive to composition and temperature changes, we have taken advantage of the progress made over the years, by us and others, improving the methodology of sample preparation under carefully controlled conditions, of aqueous and nonaqueous systems, the microscopes, and low-dose imaging.

Experimental

We studied the H_2O -isooctane- $C_{12}E_5$ system in the homogeneous monophasic channel from the water-rich to the oil-rich side, at increasing temperatures. We based our research on studies of the H_2O -n-octane- $C_{12}E_5$ system done in the past by Strey et al. [47] and Kahlweit et al. [44].

Microemulsions were prepared by weighing the nonionic surfactant $C_{12}E_5$, adding isooctane, and then adding water, both volumetrically.

Pentaethyleneglycol mono n-dodecyl ether ($C_{12}E_5$), 99 % pure, was purchased from Nikkol Chemicals (Tokyo, Japan). Water was purified by a Millipore Milli-Q purification system. Isooctane (2,2,4-trimethylpentane), 99 % pure, $\rho=0.692$ gr/ml, was purchased from Aldrich (Rehovot, Israel).

Stable single-phase microemulsions at a constant surfactant concentration of 7 wt% were obtained for all α values, namely, the oil-to-(water + oil) weight ratios. All solutions were transparent and were kept at proper temperature (see Table 1) to equilibrate in a thermostatic bath (Fried Electric, Haifa, Israel) for at least 4 days. To avoid compositional changes due to evaporation of isooctane and water, the samples were kept in glass vials with parafilm wrapped around the cap (Fig. 1).

Liquid ethane at its freezing point, our cryogen of choice [48], could not be used for vitrifying bicontinuous and oil-continuous microemulsions, because it dissolves oil [38]. Instead, we used liquid nitrogen at its boiling point. Liquid nitrogen gives relatively slow cooling rates, which cause normal hydrocarbons to crystallize. To overcome this problem, we replaced the n-octane in the original Kahlweit and coworkers' studies by isooctane. The branched hydrocarbon undergoes vitrification rather than crystallization even at the relatively slow cooling rates of approximately 5000 K/s given by boiling liquid nitrogen. Due to the replacement of n-octane by isooctane we expected small deviations in the phase diagram of the

Table 1 The microemulsions studied

α	5	10	20	30	40	50	60	70	80	90
T (°C)	20	25	27	32	32	33	33	34	36	37

original n-octane system [49]. Thus, we mapped the one-phase corridor in the phase diagram of isooctane-based system. Indeed, small deviations from the original system were found, as shown in Fig. 2. For our study, we selected points that lie in the modified “one-phase corridor” (Table 1).

Cryo-TEM

We prepared the cryo-specimens in a controlled environment vitrification system (CEVS). Detailed information regarding cryo-TEM is given by Talmon [41] and references therein. In brief, a drop of the sample was applied onto a carbon-coated film supported on a TEM copper grid. The drop was thinned into a film less than 300 nm thick by blotting away excess solution with filter paper wrapped on a metal strip. The grid was then plunged into the cryogen. The specimens were kept in liquid nitrogen and transferred to the microscope using an Oxford CT-3500 (Oxford Instruments, Abingdon, England) or a Gatan 626 (Gatan, Pleasanton, CA, USA) cryo-holders, cooled prior to the transfer. The specimens were examined by an FEI T12 G² TEM, using the low-dose imaging mode (no more than 20 electrons per Å²) to minimize electron-beam radiation damage. Images were recorded by a cooled-CCD US1000 camera (Gatan, Pleasanton, CA, USA).

Cryo-SEM

We prepared the cryo-specimen in a CEVS modified for cryo-SEM work. After the vitrification, the specimen was transferred into a BAF 060 system [Leica, Vienna, Austria],

fractured, and a small layer of the solvent was etched by sublimation, as the specimen was heated to -100 °C for 5 s, and cooled back to -150 °C. Then, the specimen was coated with 4-nm platinum-carbon layer. Because of the high vapor pressure of isooctane, even at very low temperatures, some sublimation took place during specimen manipulation, without additional heating [45]. The coating improves sample conductivity to avoid charging, and the sublimation helps to reveal greater details under the surface. The specimens were then transferred into the microscope using a BAL-TEC (now Leica) VCT100 transfer system. Imaging was performed in a Zeiss Ultra Plus high-resolution scanning electron microscope equipped with a Schottky field-emission gun, and fitted with a VCT100 cold-stage system. The microscope was operated at an accelerating voltage of 1 to 1.5 kV. Imaging was done by mixing signals from two detectors: the InLens detector—a high-resolution secondary electron detector located in the microscope column, and the Everhardt Thornley detector, placed on the specimen chamber. Detailed information regarding our cryo-SEM methodology is given by Issman and Talmon [44].

Results and discussion

As was stated above, the main focus of this work is direct imaging of the evolving nanostructures that form, as we go from the water-rich side to the oil-rich side of the “one-phase corridor,” one observes in the “ χ -cut” of the of the isooctane-water-C₁₂E₅ phase diagram, namely at a constant surfactant concentration, and increasing relative amounts of oil and of temperature (Fig. 1). Those nanostructures were previously described mainly on the basis of indirect methods. Here, we used cryo-TEM and cryo-SEM across the entire single-phase microemulsion corridor of the studied systems. Because cryo-EM specimen preparation may lead to structural artifacts,

Fig. 1 The H₂O-n-octane-C₁₂E₅ (7 wt%) χ -cut phase diagram. α is the ratio of oil to oil-plus-water in the system. Redrawn after [49]

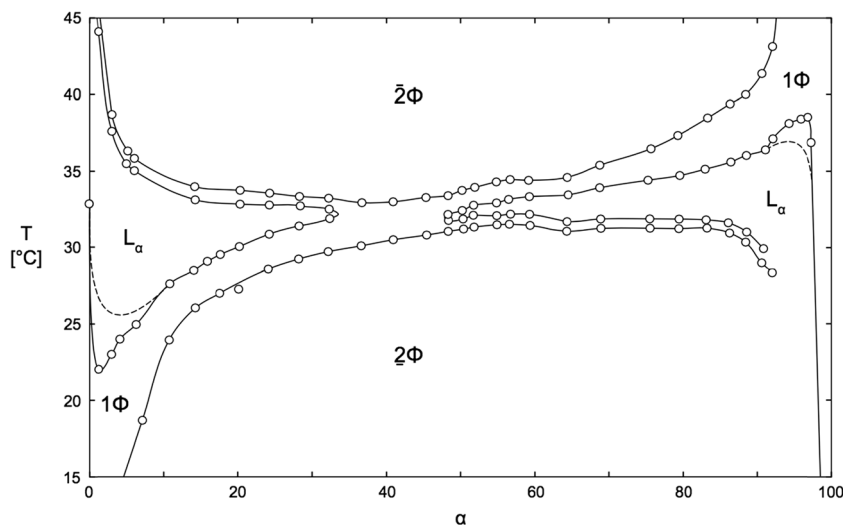
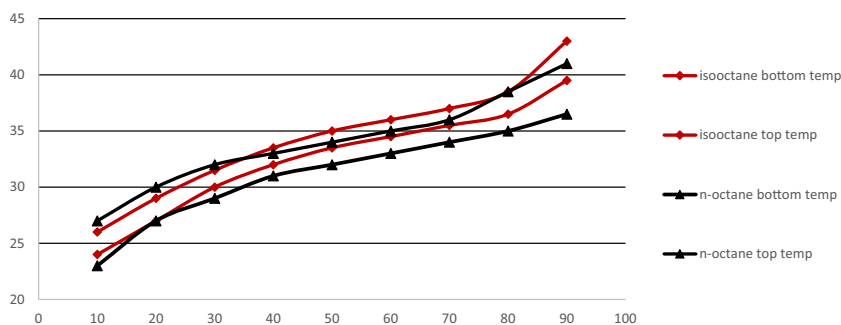


Fig. 2 The “one-phase corridor” in the octane-based (black) and the isooctane-based (orange) phase diagrams (see text). Vertical axis is the temperature in °C; the horizontal axis is α . Compare to Fig. 1

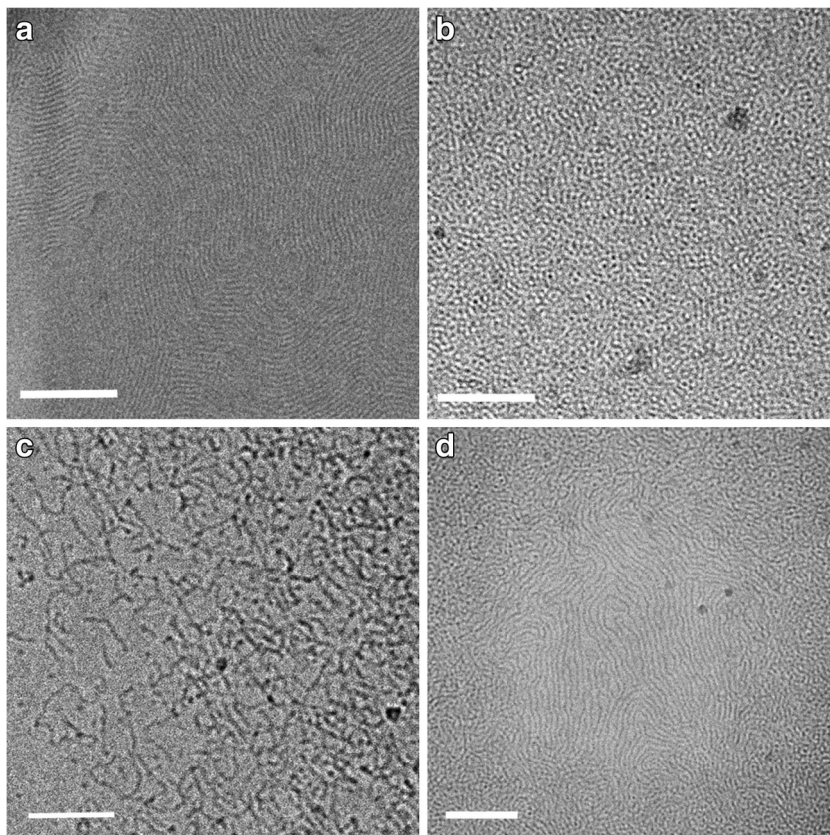


using more than one methodology leading to the same results adds credibility to the imaging of those very labile systems. Only in systems of low α values, cryo-SEM imaging is not practicable, because of the very small dimensions of the swollen micelles present in those systems, and the difficulty of vitrifying the relatively thick specimens needed for cryo-SEM, when the sample is water-rich.

Figure 3a, b show cryo-TEM images of the system at $\alpha = 5\%$. Figure 3a shows a very thin area, in which the threadlike micelles (TLMs) were aligned into ordered domains as a result of the shear and the thinning of the specimen during the blotting of the microemulsion drop on the perforated carbon film,

prior to plunging into the cryogen, liquid ethane at its freezing point, in this case. This type of specimen preparation artifact is well documented. It was observed already many years ago with surfactant in water TLMs [50] and more recently in the isooctane-water-lecithin system, where the micelles are inverted TLMs [51]. When the specimen is rather thick and the TLMs not aligned, it is impossible to tell TLMs from spheroidal micelles because of the projection of many micelles on the CCD detector. That, too, was shown by Koifman et al. [51]. We should add that those nanostructures had been shown for a similar system quite some time ago, as those were approachable by cryo-TEM from the 1980s [41].

Fig. 3 Cryo-TEM images of water-continuous systems; 7 wt% $C_{12}E_5$; **a**, **b** $\alpha = 5\%$ and $T = 20^\circ\text{C}$; a thin area showing aligned TLMs in **a** and a thick area of superposed TLMs in **b**; **c** $\alpha = 10\%$ and 25°C . The thin area at the left-hand side shows a few shorter TLMs. The area on the right is much thicker, showing many superposed TLMs. **d** $\alpha = 15\%$ and $T = 29^\circ\text{C}$. The thin area in the center shows a single layer of TLMs, while the edges show thicker areas of many superposed TLMs (bars are 100 nm)



We were able to image individual TLMs in the $\alpha=10\%$ system, where the specimen showed variable thickness, shear was moderate, and the TLMs relaxed to their native state, following thinning of the liquid, and before quenching into the cryogen (Fig. 3c). That image shows the differences one sees between thin and thick areas of the cryo-TEM specimens. In the thin area (left), there are few and shorter TLMs, while in the thicker areas, there are more numerous and longer micelles. In fact, in the far right of the micrograph, it is quite difficult to tell what is the nanostructure of the aggregates due to superposition of many TLMs, all projected in-focus on the detector of the CCD camera. Figure 3d shows a cryo-TEM image of the system at $\alpha=15\%$. In the center, we observe long TLMs in a thin layer of vitreous ice. In the edges, the specimen is thicker and many TLMs are projected, superposed, on the detector, preventing identification of the TLM nanostructure. With this system, too, we were not able to obtain good cryo-SEM pictures, due to water freezing artifacts.

At $\alpha=20\%$ and $30\text{ }^\circ\text{C}$, the micrographs collected by cryo-TEM and cryo-SEM show a very different structure as compared to the previous compositions. Instead of individual swollen micelles, both methodologies indicate that the system has gone toward a bicontinuous structure. While imaging alone is insufficient to determine whether the system has actually passed the percolation threshold, the micrographs do suggest that system is very close to it. While we have not measured the exact “percolation threshold” of this system, the α value is quite reasonable compared to other systems, where values of about 25 wt% water are quoted as typical [52].

In comparing the cryo-TEM micrograph in Fig. 4a to the cryo-SEM picture of Fig. 4b, one should take into account what is actually imaged, and how. As mentioned above, the cryo-TEM micrograph is a projection of the entire relatively thin specimen onto the CCD camera detector. Because of the optics of the TEM, all the information in the specimen is projected in-focus on the detector, which could make image interpretation difficult. That difficulty could be overcome by electron tomography, which we have not used in this study.

In the cryo-TEM images of this system, e.g., Fig. 4a, the network of branched oil-swollen TLMs are seen at relatively high contrast relative to the water domains. The good contrast is probably due to the tight packing of oil molecules within the micelles, and to the surfactant layer separating the oil-rich and water-rich domains. The superposition of the structures makes it quite difficult to assess the actual size of the water domains, which appear smaller in projection than their real size.

Cryo-SEM shows the fracture surface of the thermally fixed specimens; thus, what we see in the picture is quite different from what we see the cryo-TEM images. Note that a distinction is made here between the cryo-SEM picture, which is not formed by an optical system, and the cryo-TEM image, which is formed optically. The lighter domains seen in Fig. 4b are fractured thermally fixed water domains. The cavities around them were originally filled with isooctane. Because isooctane has an appreciable vapor pressure even at cryogenic temperatures, much of it sublimates during the transfer of the cryo-specimen from where it is prepared to the cooling holder of the SEM, and during the final cooldown to the work temperature, below $-140\text{ }^\circ\text{C}$. That sublimation, which does not affect the water domains, gives the excellent picture (topographic) contrast we see in Fig. 4b. Ben-Barak and Talmon [45] discussed in more detail the partial sublimation of isooctane from cryo-SEM specimens.

We then examined the microemulsions at $\alpha=40, 50,$ and 60% . All those show clearly bicontinuous structures, but the water and oil domains are similar in size in this α range. Figure 5a, b show cryo-EM micrographs of the system at $\alpha=40\%$ and $T=34\text{ }^\circ\text{C}$. The bicontinuous nature of these systems is quite clear here. As explained above, cryo-TEM and cryo-SEM micrographs give the same information, but shown differently due to the different mechanisms of image or picture formation by the two very different types of microscopes. Very similar structures are seen at $\alpha=50\%$ and $T=34\text{ }^\circ\text{C}$ (not shown) and at $\alpha=60\%$ and $T=36\text{ }^\circ\text{C}$, as seen in Fig. 5c, d. However,

Fig. 4 Cryo-EM micrographs of the system at $\alpha=20\%$ and $30\text{ }^\circ\text{C}$, 7 wt% C_{12}E_5 ; cryo-TEM (a) and cryo-SEM (b). Bars are 100 nm

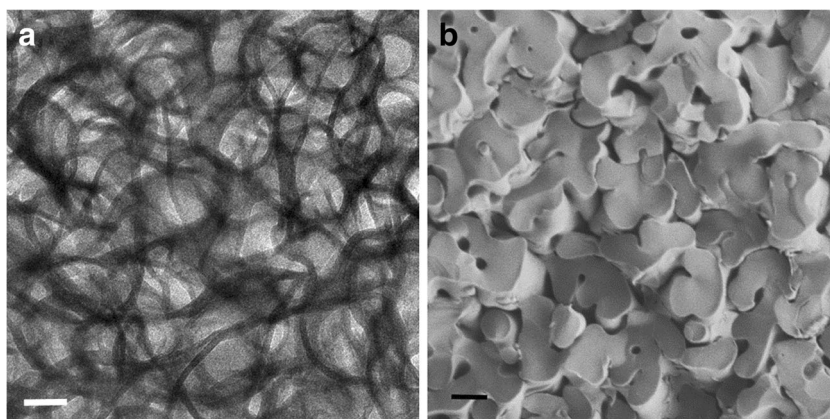
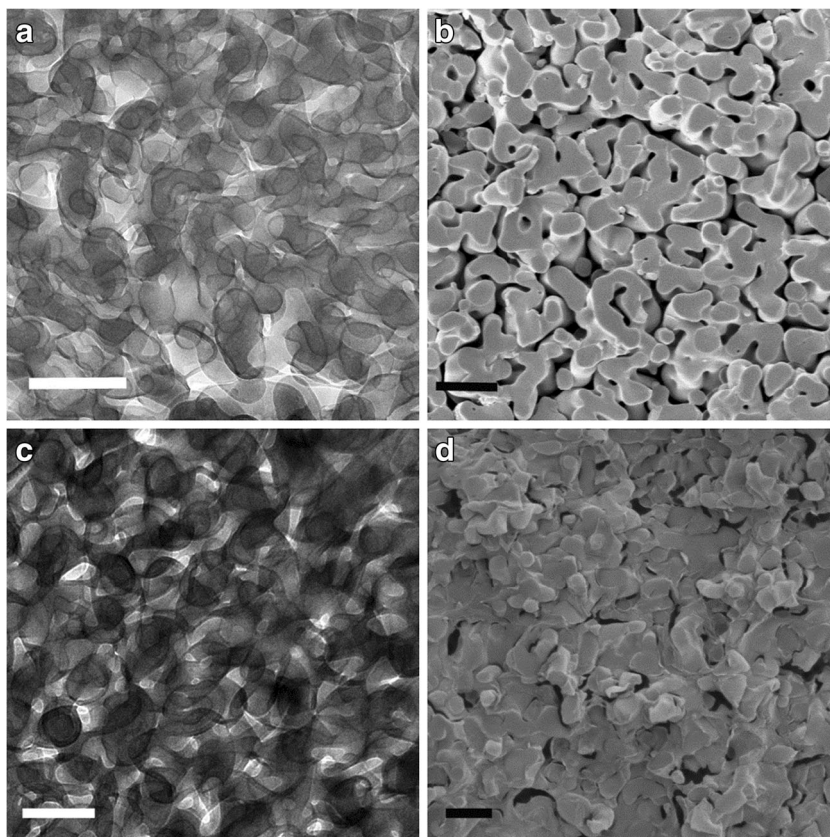


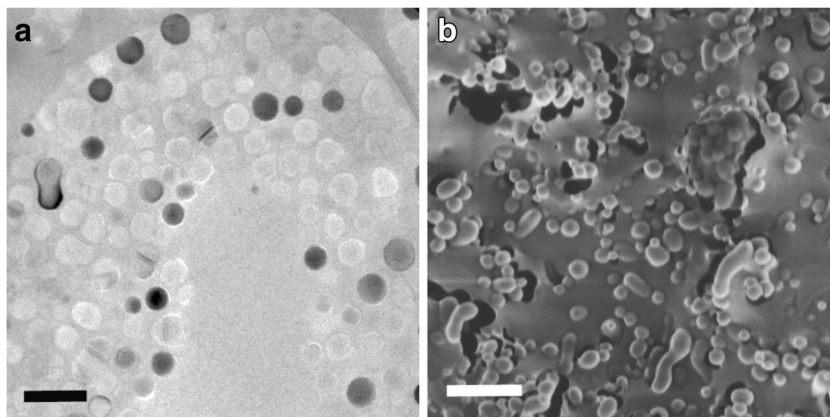
Fig. 5 Cryo-EM micrographs of the system, 7 wt% $C_{12}E_5$, at $\alpha=40\%$ and $34\text{ }^\circ\text{C}$ (**a, b**), and 60% and $36\text{ }^\circ\text{C}$ (**c, d**). The micrographs shown in **a** and **c** are of cryo-TEM, and those in **b** and **d** are cryo-SEM. Bars are 200 nm (**a**), 500 nm (**b**), 200 nm (**c**), and 400 nm (**d**)



in the latter case, although the structure is still bicontinuous, it has changed. The water domains are now smaller and tend to break their continuity. That is seen better in the picture of the fractured frozen specimen (cryo-SEM). The difference in void size in the cryo-SEM picture is related to the amount of oil sublimated from the specimen. This partial sublimation is not well controlled, as it depends on the local temperature history of the specimen. It is hard to obtain reliable quantitative data out of such micrographs. Such data is best obtained from scattering methods, relying for data interpretation on the nanostructure building blocks as elucidated by the electron microscopy.

At $\alpha=70\%$ and higher, the system becomes oil-continuous. The higher the oil content is, the smaller are the water domains. Also in this part of the one-phase corridor of the phase diagram, we can apply both cryo-TEM and cryo-SEM to image directly the nanostructures formed at any given α and temperature. We used a branched oil in this study, and the thermal fixation was performed in liquid nitrogen, but the continuous oil vitrified even by the low cooling rates provided by the boiling nitrogen, while the isolated small water domains were actually frozen (crystallized). This is best observed in the cryo-TEM image (Fig. 6a). The system here is at $\alpha=80\%$ and $T=36\text{ }^\circ\text{C}$.

Fig. 6 Cryo-TEM (**a**) and cryo-SEM (**b**) of the system at $\alpha=80\%$ and $T=36\text{ }^\circ\text{C}$, 7 wt% $C_{12}E_5$. Bars correspond to 500 nm



That the water domains are indeed crystallized is obvious from the contrast, which varies from one ice domain to another, due to their different positions with respect to the electron beam. The crystals whose positions satisfy Bragg's law of diffraction appear dark, while those who do not appear light. Defects in the ice crystals are apparent as dark and light bands [53]. Note also a swollen micelle about to split (left-hand side of micrograph). The cryo-TEM image shows an area that is very thin in its center and thicker at its edges. Note that the swollen inverted micelles were pushed from the thin area into the thicker areas around it.

The cryo-SEM pictures of the same system, Fig. 6b, corroborate the findings of the cryo-TEM images. Again, we should keep in mind that those show the surface of the fracture surface of a vitrified specimen. The water domains here appear as blobs of lighter rims, because those domains give rise to more secondary electrons than the thicker ones, as the electron beam generates secondary electrons on entering and leaving the particles. Note here, too, the size distribution and the occasional water domain made of two or three fused swollen micelles.

This is the first report of a complete direct-imaging nanostructural mapping that follows the entire spectrum of microemulsion evolution, from oil-in-water ME through the gradual development into a bicontinuous ME, and then the breakup into water-in-oil ME. Taking advantage of the current state of the technology, we were able to apply in most of the systems both cryo-TEM and cryo-SEM specimen preparation and imaging methodologies, which have supported each other's findings.

Conclusions

The goal of direct-imaging microemulsions has been the "Holy Grail" of ME research, in the words of the late L.E. "Skip" Scriven, a pioneer in the study of MEs, and the first to envision the gradual, smooth transition from oil-in-water to water-in-oil MEs, through bicontinuous MEs [2]. By judicious and careful application of a combination of cryo-TEM and cryo-SEM, we have been able to map this spectrum of nanostructures in the water- $C_{12}E_5$ -isooctane ternary system, showing the exact string of nanostructural events, as predicted in the mid-1970s for such systems. The system in the focus of this paper has been studied extensively by many over the years, as we described above. There has been also an excellent nanostructural study by freeze-fracture-replication of this system [33], but that one, although in retrospect it provided the correct answers, left uncertainties as for the control of the system conditions during specimen preparation and picture interpretation. In our study, we used state-of-the-technology cryo-EM methodologies that assured accurate control of

the ME composition and temperature. The two truly direct imaging techniques were used in parallel, thus giving more credence to the micrographs we obtained, and to the nanostructures we deduced from them. This approach, described here in full for the first time, will be used in the study of many other complex liquid systems.

Acknowledgments Our work on microemulsions has been supported by a grant from the Israel Science Foundation (ISF). The cryo-EM work was performed at the Laboratory for Electron Microscopy of Soft Matter, supported by the Technion Russell Berrie Nanotechnology Institute (RBNI). The authors thank Dr. Ellina Kesselman and Ms. Judith Schmidt for help with some of the cryo-TEM work.

References

1. Hoar TP, Schulman JH (1943) Transparent water-in-oil dispersions: the oleopathic hydro-micelle. *Nature* 152:102–3
2. Scriven LE (1976) Equilibrium bicontinuous structure. *Nature* 263:123–5
3. Danielsson I, Lindman B (1981) The definition of microemulsion. *Colloid Polym Sci* 3:391–2
4. Friberg SE (1982) Comments on "the definition of microemulsion". *Colloids Surf A* 2:201
5. Evans DF, Wennerström H (1999) *The colloidal domain*, 2nd edn. Wiley-VCH, New York
6. Komura S (2007) Mesoscale structures in microemulsions. *J Phys Condens Matter* 19:463101
7. Chen SJ, Evans DF, Ninham BW (1984) Properties and structure of three-component ionic microemulsions. *J Phys Chem* 88:1631–4
8. Lin T-L, Liu C-C, Roberts MF, Chen S-H (1991) Structure of mixed short-chain lecithin/long-chain lecithin aggregates studied by small-angle neutron scattering. *J Phys Chem* 95:6020–7
9. Fontell K, Ceglie A, Lindman B, Ninham B (1986) Some observations on phase diagrams and structure in binary and ternary systems of didodecyltrimethylammonium bromide. *Acta Chem Scand* 40:247–56
10. Lenz U, Hoffmann H (1992) Dynamic behavior of ternary microemulsions consisting of didodecyltrimethylammoniumbromide, water and hydrocarbon. *Ber Bunge Ph Chem* 96:809–15
11. Sottmann T, Stubenrauch C (2009) Phase behavior, interfacial tension and microstructure of microemulsions. In: Stubenrauch C (ed) *Microemulsions: background, new concepts, applications, perspectives*. John Wiley & Sons, Ltd, Oxford, pp 1–47
12. Sottmann T, Strey R (2005) Microemulsions. In: Lyklema J (ed) *Fundamentals of interface and colloid science*. Elsevier, Amsterdam, pp 1–96
13. Lichterfeld F, Schmeling T, Strey R (1986) Microstructure of microemulsions of the system water-n-tetradecane-alkyl polyglycol ether ($C_{12}E_5$). *J Phys Chem* 90:5762–6
14. Stubenrauch C, Sottmann T (2009) *Microemulsions stabilized by sugar surfactants in sugar-based surfactants: fundamentals and application*. C.C. Ruiz (ed.), CRC Press/Taylor & Francis, Boca Raton
15. Wolf L, Hoffmann H, Talmon Y, Teshigawara T, Watanabe K (2010) Cryo-TEM imaging of a novel microemulsion system of silicone oil with an anionic/nonionic surfactant mixture. *Soft Matter* 6:5367
16. Yaron PN, Reynolds PA, McGillivray DJ, Mata JP, White JW (2010) Nano- and microstructure of high-internal phase emulsions under shear. *J Phys Chem B* 114:3500–9

17. Kahlweit M, Lessner E, Strey R (1983) Influence of the properties of the oil and the surfactant on the phase behavior of systems of the type water–oil–nonionic surfactant. *J Phys Chem* 87:5032–40
18. Arleth L, Pedersen JS (2001) Droplet polydispersity and shape fluctuations in AOT [bis(2-ethylhexyl)sulfosuccinate sodium salt] microemulsions studied by contrast variation small-angle neutron scattering. *Phys Rev E: Stat Phys Plasmas, Fluids* 63:061406–1
19. Hirasaki GJ, Miller CA, Puerto M (2008) Recent advances in surfactant EOR. International Petroleum Technology Conference, IPTC 2008, December 3, 2008 - December 5. *Soc Petrol Eng* 1: 130–64
20. Puerto M, Hirasaki GJ, Miller CA, Barnes JR (2010) Surfactant systems for EOR in high-temperature, high-salinity environments. 17th SPE Improved Oil Recovery Symposium, IOR 2010, April 24, 2010 - April 28. *Soc Petrol Eng (SPE)* 1:356–75
21. Spermath A, Aserin A (2006) Microemulsions as carriers for drugs and nutraceuticals. *Adv Colloid Interface Sci* 128–130:47–64
22. Lutter S, Tiersch B, Koetz J, Boschetti-de-Fierro A, Abetz V (2007) Covalently closed microemulsions in presence of triblock terpolymers. *J Colloid Interface Sci* 311:447–55
23. Gayet F, Kalamouni CE, Lavedan P, Marty J, Brulet A, Viguier NL (2009) Ionic liquid/oil microemulsions as chemical nanoreactors. *Langmuir* 25:9741–50
24. Kim D, Oh S, Lee J (1999) Preparation of ultrafine monodispersed indium-tin oxide particles in AOT-based reverse microemulsions as nanoreactors. *Langmuir* 15:1599–603
25. Eastoe J, Hollamby MJ, Hudson L (2006) Recent advances in nanoparticle synthesis with reversed micelles. *Adv Colloid Interface Sci* 128–130:5–15
26. Talmon Y, Adrian M, Dubochet J (1986) Electron beam radiation damage to organic inclusions in vitreous, cubic, and hexagonal ice. *J Microscopy* 141:375–84
27. Kunieda H, Shinoda K (1982) Phase behavior in systems of nonionic surfactant/water/oil around the hydrophile-lipophile-balance temperature (HLB temperature). *J Dispersion Sci Technol* 3:233–44
28. Olsson U, Shinoda K, Lindman B (1986) Change of the structure of microemulsions with the hydrophile-lipophile balance of nonionic surfactant as revealed by NMR self-diffusion studies. *J Phys Chem* 90:4083–8
29. Kahlweit M, Strey R (1986) Phase behavior of quinary systems water-oil-nonionic amphiphile-ionic amphiphile-electrolyte. *J Phys Chem* 90:5239–44
30. Talmon Y (1983) Staining and drying-induced artifacts in electron microscopy of surfactant dispersions. *J Colloid Interface Sci* 93: 366–82
31. Bellare JR, Davis HT, Scriven LE, Talmon Y (1988) Controlled environment vitrification system: an improved sample preparation technique. *Microsc Res Tech* 10:87–111
32. Uhlmann DR (1972) A kinetic treatment of glass formation. *J Non-Cryst Solids* 7:337–48
33. Jahn W, Strey R (1988) Microstructure of microemulsions by freeze fracture electron microscopy. *J Phys Chem* 92:2294–301
34. Talmon Y (2007) Seeing giant micelles by cryogenic-temperature transmission electron microscopy (Cryo-TEM). In: Zana R, Kaler EA (eds) *Giant micelles*. CRC Press, New York, pp 163–178
35. Cui H, Hodgdon TK, Kaler EW, Abezgauz L, Danino D, Lubovsky M, Talmon Y, Pochan DJ (2007) Elucidating the assembled structure of amphiphiles in solution via cryogenic transmission electron microscopy. *Soft Matter* 3:945–55
36. Zhong S, Pochan DJ (2010) Cryogenic transmission electron microscopy for direct observation of polymer and small-molecule materials and structures in solution. *J Macromol Sci Polym Rev* 50:287–320
37. Oostergetel GT, Esselink FJ, Hadziioannou G (1995) Cryo-electron microscopy of block copolymers in an organic solvent. *Langmuir* 11:3721–4
38. Danino D, Gupta R, Satyavolu J, Talmon Y (2002) Direct cryogenic-temperature transmission electron microscopy imaging of phospholipid aggregates in soybean oil. *J Colloid Interface Sci* 249:180–6
39. Davis VA, Parra-Vasquez ANG, Green MJ, Rai PK, Behabtu N, Prieto V, Booker RD, Schmidt J, Kesselman E, Zhou W, Fan H, Adams WW, Hauge RH, Fischer JE, Cohen Y, Talmon Y, Smalley RE, Pasquali M (2009) True solutions of single-walled carbon nanotubes for assembly into macroscopic materials. *Nat Nanotechnol* 4:830–4
40. Behabtu N, Lomeda JR, Green MJ, Higginbotham AL, Sinitkii A, Kosynkin DV, Tsentelovich D, Parra-Vasquez ANG, Schmidt J, Kesselman E, Cohen Y, Talmon Y, Tour JM, Pasquali M (2010) Spontaneous high-concentration dispersions and liquid crystals of graphene. *Nat Nanotechnol* 5:406–11
41. Bernheim-Groswasser A, Tlustý T, Safran SA, Talmon Y (1999) Direct observation of phase separation in microemulsion networks. *Langmuir* 15:5448–53
42. Note C, Ruffin J, Tiersch B, Koetz J (2007) The influence of polyampholytes on the phase behavior of microemulsion used as template for the nanoparticle formation. *J Dispersion Sci Technol* 28:155–64
43. Note C, Koetz J, Kosmella S (2006) Structural changes in poly(ethyleneimine) modified microemulsion. *J Colloid Interface Sci* 302:662–8
44. Issman L, Talmon Y (2012) Cryo-SEM specimen preparation under controlled temperature and concentration conditions. *J Microsc* 246:60–69
45. Ben-Barak I, Talmon Y (2012) Direct-imaging cryo-SEM of nanostructure evolution in didodecyl-dimethylammonium bromide-based microemulsions. *Z Phys Chem* 226:665–674
46. Kleinerman O, Parra-Vasquez AN, Green MJ, Behabtu N, Schmidt J, Kesselman E, Young CC, Cohen Y, Pasquali M, Talmon Y (2015) Cryogenic-temperature electron microscopy direct imaging of carbon nanotubes and graphene solutions in superacids. *J Microsc* 259:16–25
47. Kahlweit M, Strey R (1985) Phase behavior of ternary systems of the type H₂O-oil-nonionic amphiphile microemulsions. *Angew Chem Int Ed Engl* 24:654–668
48. Talmon Y (2015) The study of nanostructured liquids by cryogenic-temperature electron microscopy- A status report. *J Mol Liq* 210 (Part A):2–8
49. Kahlweit M, Strey R, Haase D et al (1987) How to study microemulsions. *J Colloid Interface Sci* 118:436–453
50. Clausen TM, Vinson PK, Minter JR, Davis HT, Talmon Y, Miller WG (1992) Viscoelastic micellar solutions: microscopy and rheology. *J Phys Chem* 96:474–484
51. Koifman N, Schnabel-Lubovsky M, Talmon Y (2013) Nanostructure formation in the lecithin/ isooctane/water System. *J Phys Chem B* 117:9558–9567
52. Fanun M (2009) Microemulsions, properties and applications. In: *Surfactant Science Series vol. 144*. CRC Press, Boca Raton, p 110
53. Wolf L, Hoffmann H, Teshigawara T, Okamoto T, Talmon Y (2012) Microemulsions with a HIPME structure. *J Phys Chem B* 116: 2131–2137